Makkonen, Ilja; Korhonen, Esa; Prozheeva, Vera; Tuomisto, Filip

Identification of vacancy defect complexes in transparent semiconducting oxides ZnO, In_2O_3 and SnO_2

Published in:
Journal of physics: Condensed matter

DOI:
10.1088/0953-8984/28/22/224002

Published: 08/03/2016

Document Version
Peer-reviewed accepted author manuscript, also known as Final accepted manuscript or Post-print

Please cite the original version:
Makkonen, I., Korhonen, E., Prozheeva, V., & Tuomisto, F. (2016). Identification of vacancy defect complexes in transparent semiconducting oxides ZnO, In_2O_3 and SnO_2. *Journal of physics: Condensed matter*, *28*(22), 1-7. Article 224002. https://doi.org/10.1088/0953-8984/28/22/224002

Identification of vacancy defect complexes in transparent semiconducting oxides: the cases of ZnO, In_2O_3 and SnO_2

Ilja Makkonen, Esa Korhonen, Vera Prozheeva and Filip Tuomisto

Department of Applied Physics, Aalto University School of Science, P.O. Box 14100, FI-00076 Aalto, Espoo, Finland

E-mail: ilja.makkonen@aalto.fi

Abstract. Positron annihilation spectroscopy, when combined with high-quality supporting modeling of positron states and annihilation in matter, is a powerful tool for detailed defect identification of vacancy-type defects in semiconductors and oxides. Here we demonstrate that the Doppler broadening of the positron annihilation radiation is a very sensitive means for observing the oxygen environment around cation vacancies, the main open-volume defects trapping positrons in measurements made for transparent semiconducting oxides. Changes in the positron annihilation signal due to external manipulation such as irradiation and annealing can be correlated with the associated changes in the sizes of the detected vacancy clusters. Our examples for ZnO, In_2O_3 and SnO_2 demonstrate that oxygen vacancies in oxides can be detected directly using positron annihilation spectroscopy when they are complexed with cation vacancies.

Submitted to: *J. Phys.: Condens. Matter*

1. Introduction

Transparency and conductivity are usually mutually exclusive material properties since transparency to visible light requires an optical band gap of around 3 eV which generally implies insulating instead of semiconducting material. One material category with these properties is the so-called transparent semiconducting oxides (TSOs). In the case of TSOs the conductivity is caused by shallow donor states, which do not significantly influence the band gap or absorb light. These states are often attributed to oxygen vacancies due to both experimental and theoretical results [1]. The most common TSOs in practical use are In_2O_3, SnO_2, ZnO and β-Ga_2O_3.

For current typical electronic applications, these materials are heavily n-doped and called transparent conducting oxides (TCOs) due to the metal-like high conductivity. In this form these materials find applications in fields such as flat-panel displays and photovoltaics [2]. TCOs are typically used as simple transparent contacts and the requirements for material quality are equally simple; high conductivity and transparency. The most common TCO in industrial use is heavily Sn-doped In_2O_3 (ITO) mainly due to its high conductivity [3].

Without degenerate doping, these materials are called transparent semiconducting oxides (TSOs), being wide band-gap semiconductors and insulating in their perfectly stoichiometric form. The current interest in these materials is fueled by their possible use in semiconductor devices. If the electrical properties of TSOs could be controlled similarly to e.g. silicon, a range of transparent electronics would become possible [4]. So far, however, the high effect of impurities and native defects on conductivity has inhibited the use of these oxides as semiconducting materials.

Positron annihilation spectroscopy is a powerful method for detection, quantification and identification of open-volume defects in solids [5]. On one hand, positrons are sensitive to vacancy defects where they easily get trapped at due to reduced repulsion of positive nuclei, but on the other hand, other point defects, extended defects or impurities do not complicate measurements. The sensitivity range for vacancies is in the technologically relevant regime of 10^{16}–10^{19} cm^{-3}. One can study both thin films and bulk, and the samples can equally well be insulating as conducting. Measuring positron lifetimes gives an indication on the sizes of open volumes within the sample, whereas the most powerful technique for true defect identification, Doppler broadening, measuring the momenta of annihilating electron-positron pairs via the Doppler broadening of the 511 keV annihilation line, also can reveal dopant or impurity atoms around vacancies. Recently, the combination of experiments and computational modeling has enabled also the investigation of even more subtle effects in measured spectra, for instance due to clustering of small N vacancies with In vacancies in InN [6] or due to open-volume defects with very small open volume trapping the positron, such as at a substitutional Li on Zn site in ZnO [7]. The close collaboration between experiment and theory has significantly advanced the capability to interpret the results of positron annihilation experiments during recent years [5]. In the present article our focus is in obtaining a better understanding of recent positron annihilation experiments made on transparent semiconducting oxides [8, 9] by combining them with first-principles calculations of measurable positron annilation parameters [10] for a more detailed defect identification. Our results and their comparison with experiments will also help to highlight the sensitivity of the Doppler broadening to the oxygen environment in oxides and establish positron annihilation as a tool being able to detect directly oxygen vacancies as complexed to cation vacancies with a larger open volume for the positron to trap to.

The structure of the present paper is as follows. In Sec. 2 we introduce some of our main ideas on the sensitivity and applicability of positron annihilation methods, especially Doppler broadening, in the identification of open-volume defects in transparent semiconducting oxides and more generally in oxides. We emphasize the sensitivity of the measured Doppler broadening on the number of oxygen ions surrounding the annihilation site. In Sec. 3 we discuss the relevant details of our positron annihilation experiments and the modeling of positron states and annihilation performed in the present work. Section 4 uses modeling to analyze trends seen in recent positron measurements of ZnO, In_2O_3 and SnO_2, and better identify the open-volume defects detected in the measurements. Finally, Sec. 5 summarizes this paper and its conclusions.

2. Positrons in the study of transparent semiconducting oxides

Although one cannot completely rule out positron trapping to isolated oxygen vacancies in oxides in general, their open volume available for the positron is nevertheless rather small, in general too small to possess a bound positron state. Also, quite often the oxygen vacancies can be expected to be positively charged, in which case the trapping rate can be expected to be much smaller that the positron annihilation rate [11]. Therefore, the positron annihilation technique is mostly sensitive to cation vacancies and similarly sized neutral or negative open volumes in oxides. However, as will be discussed below, oxygen vacancies can be directly detected when they are complexed with cation vacancies in comparable concentrations.

Once trapped at cation vacancy like defects the positron is mostly in contact with surrounding oxygen ions and most likely to annihilate with electrons on their outer atomic/ionic shells. As an example, Fig. 1 shows how each shell is expected to contribute to the Doppler broadening according to computational modeling, in the case of cation vacancies in ZnO, In_2O_3, SnO_2 as well as in a more extreme example of $SrTiO_3$, in which the coordination number reaches 12 for the Sr vacancy. The results in this particular figure have been calculated within the so-called atomic-superposition approximation [12, 13] (non-selfconsistent electron density and Coulomb potential from superposition of neutral free atoms) enabling the decomposition to be made also for valence shells. Apart from the case of ZnO with only 4 small O ions in front of larger Zn cations, in which the annihilation with the high-momentum shell Zn 3*d* is significant, the annihilation in the high-momentum part of the spectrum ($p > 1$ a.u.) is primarily with electrons on the O 2*p* shells. Therefore the shape of the spectrum typically correlates with the (average) number of O ions surrounding the positrons' annihilation sites. As will be discussed below, this makes the positron a very sensitive probe of the oxygen environment of vacancy defects and vacancy clusters in oxides, and changes in number of oxygen ions around the trapping site for instance due to vacancy clustering resulting from growth conditions, annealing or irradiation, will affect the measurable annihilation parameters, both the positron lifetime and especially the Doppler broadening. In this paper we will focus on the latter technique, which is easier to apply in the study of thin films and more sensitive to the chemical surroundings of the positrons' trapping sites.

The shape of the annihilation line is typically characterized by two line shape parameters. The *S* parameter is proportional to the relative number of

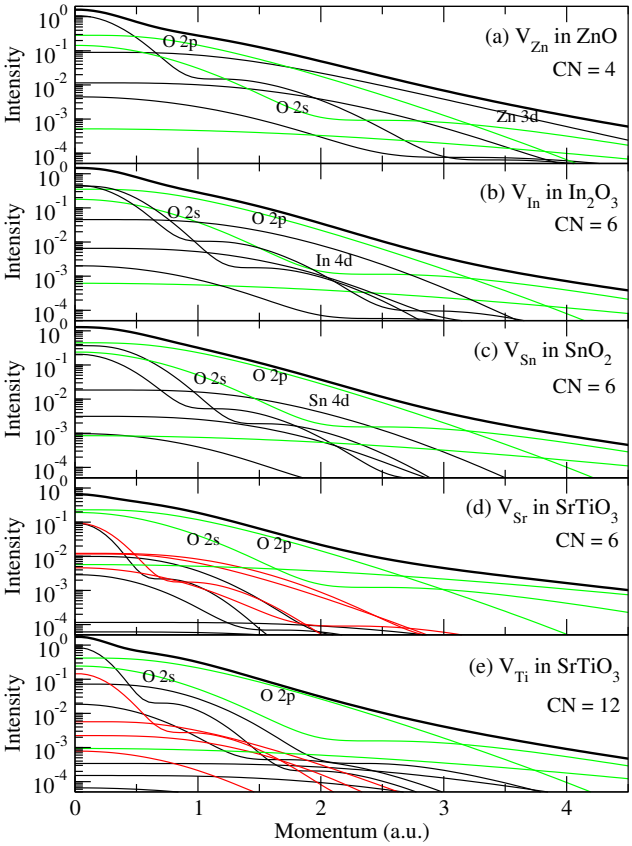

Figure 1. Decompositions of computational Doppler spectra corresponding to annihilation of localized positrons in cation vacancies in (a) ZnO, (b) In_2O_3, and (c) SnO_2, (d) V_{Sr} in $SrTiO_3$, and (e) V_{Ti} in $SrTiO_3$. The black thick line is the total spectrum, the thin green lines are the contributions of different atomic shells of oxygen, and thin black and red lines the contributions of different cation shells (A and B cations, respectively). The contributions of the shells important at high momenta, the region in which the approach used in the analysis of this figure is accurate, are labeled. CN denotes the coordination number of the cation vacancy sites.

counts in the low momentum region of the spectrum, whereas the *W* parameter describes correspondingly the intensity of the high-momentum region. Here we specify the *S* window as $|p| < 0.4$ a.u., and the *W* window as 1.6 a.u.$< |p| <$2.4 a.u. When comparing experiment with theory it is more appropriate to use relative parameters obtained by normalizing with the parameters of the lattice, $S_{\rm rel} = S/S_{\rm bulk}$ and $W_{\rm rel} = W/W_{\rm bulk}$.

The effect of vacancy clustering, i.e. having one or more oxygen vacancies ($V_{\rm O}$) clustered around cation vacancies, on the Doppler broadening of annihilation radiation is demonstrated in Fig. 2 using computational data calculated with the method described below in Sec. 3. Once trapped at a vacancy, the positron is more in contact with low-momentum valence electrons than in the delocalized bulk state. Therefore, the ratio spectra of vacancy defects assume

a value of > 1 at low momenta (S parameter window) and < 1 at high momenta (W parameter window). On average, the effect of V_O clustering is to decrease the high-momentum intensity and increase correspondingly the low-momentum one, since high-momentum O shells are removed from the surroundings of the trapping site (see Fig. 1). The specific results and trends for each material are discussed below in Sec. 4.

3. Experiments and modeling

Doppler broadening measurements were conducted using a slow positron beam, see Refs. [15, 8, 9] for details on the specific experiments discussed in this article. With such a setup, the implantation energy of positrons can be tuned in the range 0...35 keV. The mean stopping depth varies from a few nanometers up to a few micrometers. Hence low-energy positrons can be used to study near-surface layers and thin films.

Our modeling is based on the two-component density-functional theory for electron-positron systems [16]. We model the atomic and electronic structures of the bulk oxides and their defects using the supercell approximation, the projector augmented-wave method [17] as implemented in the VASP code [18, 19, 20], and the local-density approximation (LDA) [21] for the electron-electron exchange and correlation effects. We assume that the localized positron density does not affect the average electron density and use the zero-positron density limits of the electron-positron correlation potential and enhancement factor within the LDA [16]. For the wurtzite ZnO, bixbyite In_2O_3 and rutile SnO_2, we use supercells of 96, 80, and 48...162 atoms, respectively. Positron-induced forces on ions are taken into account in ionic relaxations [10]. The momentum density of annihilating electron-positron pairs is evaluated using the so-called state-dependent scheme [13] and the projector augmented-wave method [22, 10]. Prior to comparison with experiment the Doppler spectrum is convoluted with a Gaussian function corresponding to the experimental resolution function. In this work, we extract the computational (S, W) parameters by assuming a typical detector energy resolution of 1.3 keV consistent with the experimental data shown [8, 9]. The corresponding to a momentum resolution of 5.1 a.u. The resolution assumed for the full Doppler spectra in Fig. 2, 0.9 keV or 3.5 a.u., corresponds to a typical coincidence setup with 2 high-purity Ge detectors. When combined with high-quality Doppler broadening measurements, similar calculations have shown to be extermely useful in detailed defect identification [5, 10, 23, 24, 6, 7, 25].

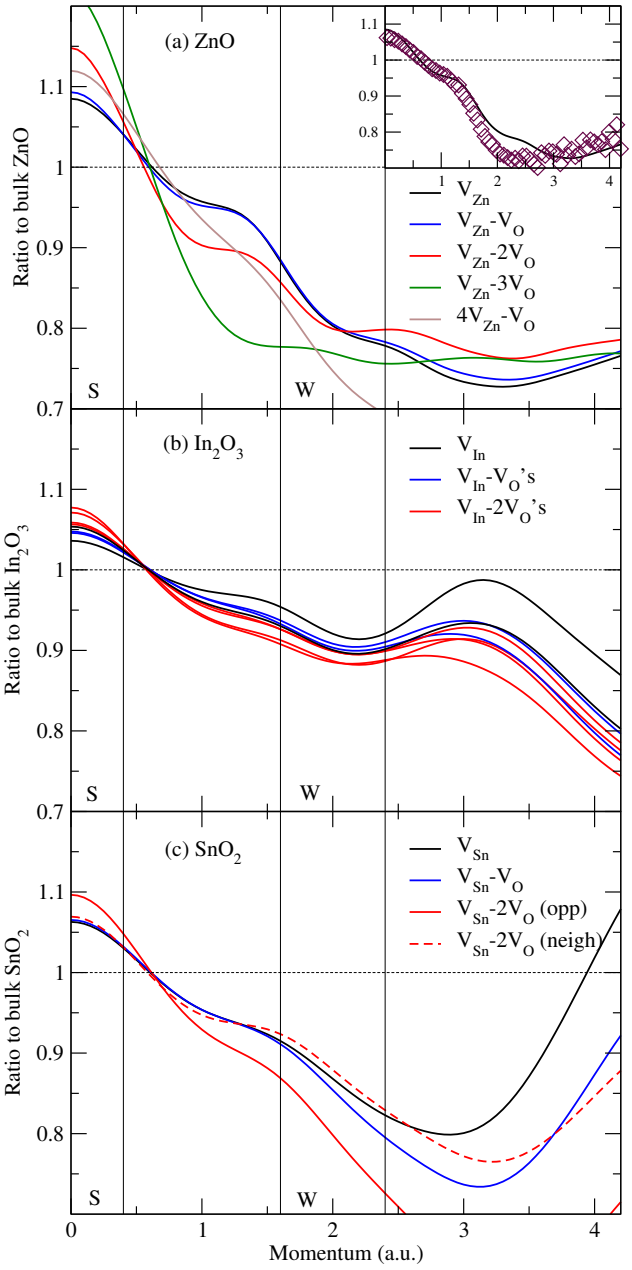

Figure 2. Computational spectra for representative defects and defect complexes in (a) ZnO, (b) In_2O_3, and (c) SnO_2. For some, several different configurations are shown. The spectra are divided by the spectrum of the corresponding defect-free lattice. The boundaries of the S and W momentum windows are shown. The inset in (a) shows a comparison with the experimental result for V_{Zn} in ZnO from Ref. [14].

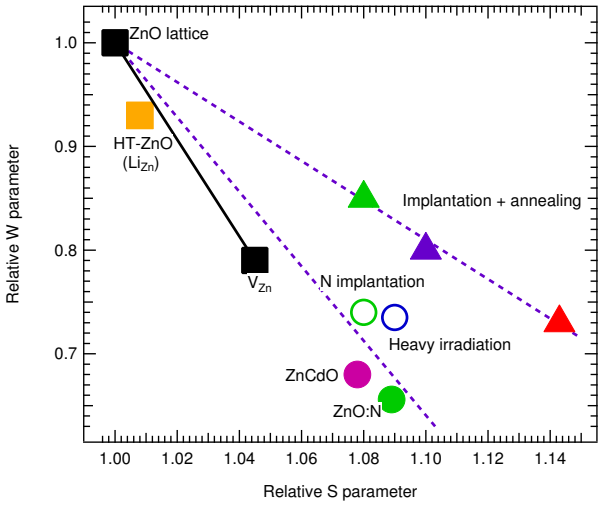

Figure 3. (S, W) plot with characteristic data from a variety of ZnO samples (reprinted from Ref. [26]). The S and W parameters are shown as normalized to those of the ZnO lattice. Reprinted with permission. Copyright Cambridge University Press.

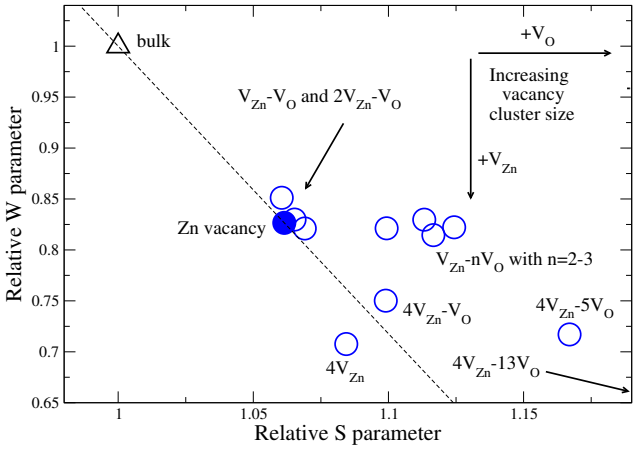

Figure 4. (S, W) plot with computational predictions for ZnO. Several different configurations for the vacancy complexes are considered. The S and W parameters are shown as normalized to those of the ZnO lattice. The $4V_{Zn}$–$13V_O$ point lies outside the limits at $(S, W) = (1.40, 0.52)$.

4. Results and discussion

4.1. ZnO

Figure 3 shows a summary of characteristic S/W values obtained from previous positron annihilation studies of ZnO (for a review, see Ref. [26]). The zinc vacancy point, V_{Zn}, measured from electron-irradiated ZnO as well as bulk reference point are from Ref. [27]. Measurement points falling on the V_{Zn}–lattice line can typically be thought to represent non-saturation trapping to V_{Zn}. A fraction of the positrons annihilates trapped at V_{Zn} and the rest in the delocalized bulk state. Points elsewhere represent defects with other identities. Li on Zn site has been shown to be a shallow positron trap with annihilation parameters close to bulk values [7]. Studies of implantation, irradiation and annealing have reported higher S and lower W values lower than those of V_{Zn} [14, 28, 29, 30, 31, 32, 33, 34, 35, 36, 37, 38, 39]. This suggests the existence of larger vacancy clusters. These points fall on two lines distinct from the V_{Zn}–lattice one suggesting the presence of two different kinds of clusters in different experiments. Combination of implantation and annealing results in higher W parameters than heavy irradiation or N implantation alone. Below we will use first-principles modeling of positron states and annihilation in vacancy defects to discuss the microscopic differences between the vacancy defects.

Figure 4 shows a theoretical point of comparison with the characteristic experimental S and W points shown in Fig. 3. We start by decorating the V_{Zn} vacancy with $1 \ldots 3$ V_O. The general trend in the data is that the (S, W) points move horizontally towards the right (increase in S) with the increasing number of V_O and decreasing number of O around the annihilation site. However, the divacancy points (V_{Zn}–V_O) still lie very close to the monovacancy one (V_{Zn}) and these two defects are practically indistinguishable. Likewise, a $2V_{Zn}$–V_O trivacancy corresponds to the same point as V_{Zn}. This is because the V_{Zn}'s are well separated and the environment sensed by the positrons is in both ends very similar to that in an isolated V_{Zn}. The V_{Zn}–nV_O points with $n = 2 \ldots 3$ are compatible with the data measured from annealed samples. In Doppler broadening these small vacancy complexes can be clearly distinguished from V_{Zn}. This would be more challenging with lifetime measurements since the spread of the lifetimes is in this case only 10–15 ps. Similarly to InN [6], in the case of vacancy complexes of ZnO the most important chemical information contained in the full coincidence Doppler spectrum [Fig. 2(a)] is actually in between the S and W momentum windows at around $p = 1$ a.u., where the O $2p$ shell dominates the spectrum [see Fig. 2(a)].

On the other hand, vacancy clusters with a larger radius (4 or more missing Zn) are needed to explain the results of implantation and irradiation studies. Figure 4 shows some representative cases [$4V_{Zn}$ and $4V_{Zn}$–V_O (two different kinds of tetrahedra bounded by Zn), $4V_{Zn}$–$5V_O$ (irregular shape), and $4V_{Zn}$–$13V_O$] whose W parameters now lie below that of V_{Zn}. Based on these predictions we expect the increase in the S parameter to be correlated with the increase in the number of oxygen vacancies in the observed clusters, whereas the data with lower W values can only be explained by having 4 or more missing Zn atoms.

4.2. In_2O_3

Korhonen *et al.* [8] have studied compensating vacancy defects in Sn and Mg doped In_2O_3 using positron annihilation. Their samples were subjected to O_2 or vacuum annealing and their effect on vacancy-type defects was studied. After the O_2 annealing, the Sn-doped samples form a line (Fig. 5, $S_{\rm defect} \geq 1.02 \times S_{\rm bulk}$, $W_{\rm defect} \leq 0.9 \times W_{\rm bulk}$) indicating a single vacancy type. The Sn concentration is not the primary factor in determining the vacancy defect concentration. After vacuum annealing the values are shifted significantly, the new span being $S_{\rm defect} \geq 1.05 \times S_{\rm bulk}$ and $W_{\rm defect} \leq 0.97 \times W_{\rm bulk}$. Since vacuum annealing is expected to remove oxygen from the samples, the obvious interpretation is that more $V_{\rm O}$ is attached to the indium vacancies. Figure 6 shows the results of our simulations. The bixbyite structure of In_2O_3 has two inequivalent In sites with differing arrangements of O around (see, for example, Ref. [40]). Each $V_{\rm In}$ has two vacancy-like "missing O" sites around and dependending on whether they are on the opposide sides of the vacancy or on the same side, the positron annihilation parameters of the two $V_{\rm In}$ are different (see again also Fig. 2(b)). Similarly, in case of $V_{\rm In}$–$nV_{\rm O}$ complexes the specific geometry and dimensionality of the open volume (linear/planar/tetrahedral) strongly affects the resulting positron annihilation parameters. However, again the Doppler broadening is more sensitive to vacancy complexing than positron lifetime. For instance, the positron lifetimes at the $V_{\rm In}$-$nV_{\rm O}$ complexes is estimated to be within a couple of picoseconds. The change in the (S, W) values due to the vacuum annealing is consistent with vacancy clusters having two or more $V_{\rm O}$ attached to $V_{\rm In}$. In conclusion, we identify the open-volume defects detected in O_2 annealed In_2O_3 in Ref. [8] as $V_{\rm In}$ and smaller vacancy complexes, whereas in vacuum annealed samples one observes vacancy complexes with at least two oxygen vacancies complexed with an indium vacancy, $V_{\rm In}$-$nV_{\rm O}$, with $n \geq 2$.

4.3. SnO_2

Korhonen *et al.* [15, 9] have studied Sb-doped thin-film SnO_2 using positron annihilation. While all their (S, W) measurement points fall on the bulk – $V_{\rm Sn}$ line or possibly on its extension beyond the $V_{\rm Sn}$ point, see Fig. 7, the samples can be divided into two different groups based on how their S parameters and conduction electron concentrations n_e are related [9]. These correspond to the two different regimes of Sb concentration depicted in Fig. 7, [Sb] $> 10^{19}$ cm^{-3} and [Sb] $< 10^{19}$ cm^{-3}. This and the rather large S values observed suggest at least two different kinds of vacancies or vacancy complexes to be behind the

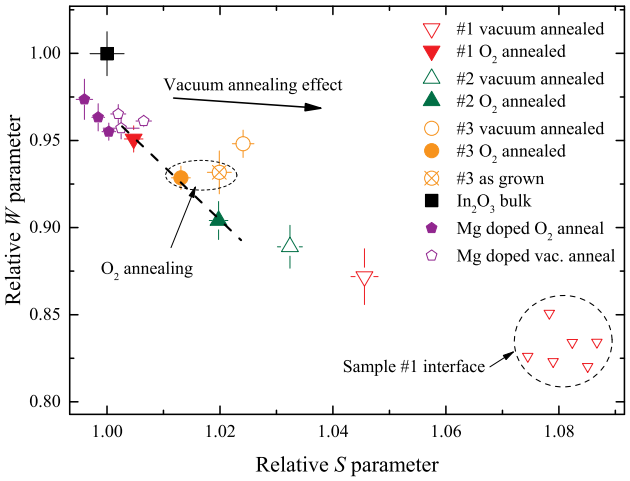

Figure 5. (S, W) plot for In_2O_3 with measured data from Ref. [8]. The S and W parameters are shown as normalized to those of the In_2O_3 lattice.

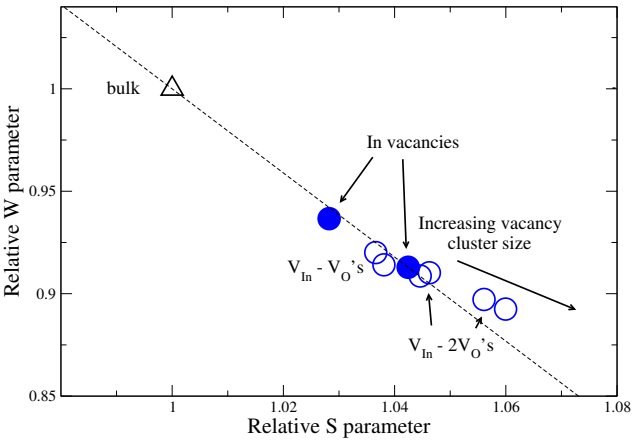

Figure 6. Computational (S, W) plot for In_2O_3. Several different configurations for the vacancy complexes are considered. The S and W parameters are shown as normalized to those of the In_2O_3 lattice.

measured data. With low [Sb]/n_e ($\sim 10^{18}$ cm^{-3}) the S parameter is above $1.05 \times S_{\rm bulk}$. This is a typical value for vacancy complexes involving at least two missing atoms. With larger Sb / conduction electron concentrations of $\geq\sim 10^{19}$ cm^{-3} the S parameter saturates to slighty below $S = 1.045 \times S_{\rm bulk}$ with increasing n_e.

We have modeled vacancies and vacancy clusters of one missing Sn in SnO_2 up to the size of a pentavacancy, $V_{\rm Sn}$–$4V_{\rm O}$, see Fig. 8. Unlike in the case of ZnO above and In_2O_3, all the points fall on the average on the extension of the bulk – $V_{\rm Sn}$ line. This supports the analysis of Korhonen *et al.* [9]. Namely, at moderate doping levels (10^{18}–10^{19} cm^{-3}) one can identify the observed defects as complexes formed of a single $V_{\rm Sn}$ and several $V_{\rm O}$. A reduction in the Sn vacancy concentration is found when the Sb

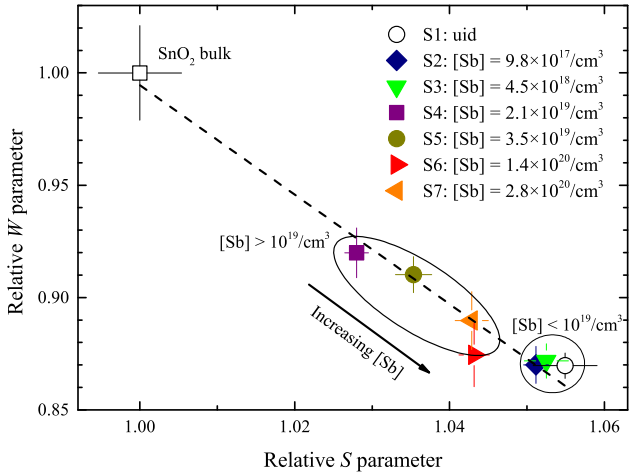

Figure 7. (S, W) plot for SnO_2 with measured data. Reprinted from Ref. [9]. The S and W parameters are shown as normalized to those of the SnO_2 lattice.

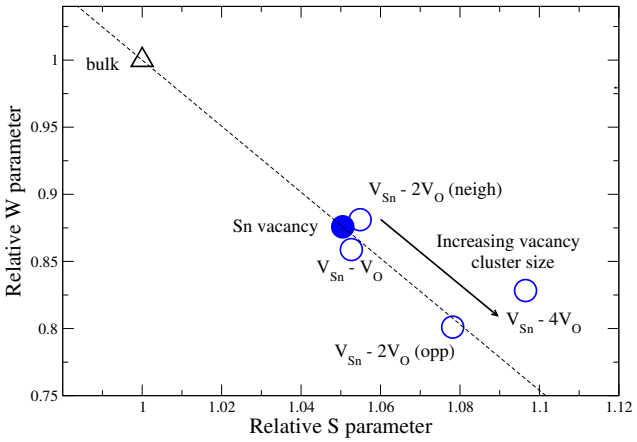

Figure 8. Computational (S, W) plot for SnO_2. The S and W parameters are shown as normalized to those of the SnO_2 lattice.

concentration is increased above 10^{19} cm^{-3}. Sb is a well-known reactive surfactanct in semiconductor thin film growth, also in case of SnO_2 [41]. The presence of Sb may significantly affect the surface mobility and cause the observed reduction in the vacancy concentration. Only once the Sb concentration clearly exceeds 10^{19} cm^{-3}, is the expected thermodynamics-driven trend seen in the Sn vacancy concentration – namely the increase of the Fermi level with increasing Sb content increases the concentration of acceptor-type Sn vacancies.

5. Summary and conclusions

In this work we have discussed the identification of vacancies and vacancy clusters in transparent semiconducting oxides using positron annihilation spectroscopy and supporting first-principles modeling and ZnO, In_2O_3 and SnO_2 as examples. We find the Doppler broadening of the 511 keV annihilation line to be extremely sensitive to the oxygen environment of the annihilation sites at open-volume defects. Addition/removal of oxygen around the annihilation sites results in observable changes of line shape parameters. Oxygen vacancies both in these systems as well as other oxides can be detected directly when they are complexed with cation vacancies large enough to be able to trap positrons. Although for many of these materials it is difficult to produce high-quality reference samples, already observing relative changes and trends in comparisons of different samples, can help to provide a defect identification, as long as their microscopic origins can be understood through modeling.

Acknowledgments

We acknowledge the generous computing resources provided by the "Aalto Science IT" project.

References

[1] King P D C and Veal T D 2011 *J. Phys.: Condens. Matter* **23** 334214 URL http://stacks.iop.org/0953-8984/23/i=33/a=334214

[2] Minami T 2008 *Thin Solid Films* **516** 5822 – 5828 URL http://www.sciencedirect.com/science/article/pii/S004060900701694X

[3] Kumar A and Zhou C 2010 *ACS Nano* **4** 11–14 URL http://dx.doi.org/10.1021/nn901903b

[4] Bierwagen O 2015 *Semicond. Science Technol.* **30** 024001 URL http://stacks.iop.org/0268-1242/30/i=2/a=024001

[5] Tuomisto F and Makkonen I 2013 *Rev. Mod. Phys.* **85**(4) 1583–1631 URL http://link.aps.org/doi/10.1103/RevModPhys.85.1583

[6] Rauch C, Makkonen I and Tuomisto F 2011 *Phys. Rev. B* **84**(12) 125201 URL http://link.aps.org/doi/10.1103/PhysRevB.84.125201

[7] Johansen K M, Zubiaga A, Makkonen I, Tuomisto F, Neuvonen P T, Knutsen K E, Monakhov E V, Kuznetsov A Y and Svensson B G 2011 *Phys. Rev. B* **83**(24) 245208 URL http://link.aps.org/doi/10.1103/PhysRevB.83.245208

[8] Korhonen E, Tuomisto F, Bierwagen O, Speck J S and Galazka Z 2014 *Phys. Rev. B* **90**(24) 245307 URL http://link.aps.org/doi/10.1103/PhysRevB.90.245307

[9] Korhonen E, Prozheeva V, Tuomisto F, Bierwagen O, Speck J S, White M E, Galazka Z, Liu H, Izyumskaya N, Avrutin V, Özgür Ü and Morkoç H 2015 *Semicond. Science Technol.* **30** 024011 URL http://stacks.iop.org/0268-1242/30/i=2/a=024011

[10] Makkonen I, Hakala M and Puska M J 2006 *Phys. Rev. B* **73**(3) 035103 URL http://link.aps.org/doi/10.1103/PhysRevB.73.035103

[11] Puska M J, Corbel C and Nieminen R M 1990 *Phys. Rev. B* **41**(14) 9980–9993 URL http://link.aps.org/doi/10.1103/PhysRevB.41.9980

[12] Puska M J and Nieminen R M 1983 *J. Phys. F: Met. Phys.* **13** 333 URL http://stacks.iop.org/0305-4608/13/i=2/a=009

[13] Alatalo M, Barbiellini B, Hakala M, Kauppinen H, Korhonen T, Puska M J, Saarinen K, Hautojärvi P and Nieminen R M 1996 *Phys. Rev. B* **54**(4) 2397–2409 URL http://link.aps.org/doi/10.1103/PhysRevB.54.2397

[14] Zubiaga A, Tuomisto F, Coleman V A, Tan H H, Jagadish C, Koike K, Sasa S, Inoue M and Yano M 2008 *Phys. Rev. B* **78**(3) 035125 URL http://link.aps.org/doi/10.1103/PhysRevB.78.035125

[15] Korhonen E, Tuomisto F, Bierwagen O, Speck J S, White M E and Galazka Z 2014 *AIP Conf. Proc.* **1583** 368–371 URL http://scitation.aip.org/content/aip/proceeding/aipcp/10.1063/1.4865672

[16] Boroński E and Nieminen R M 1986 *Phys. Rev. B* **34**(6) 3820–3831 URL http://link.aps.org/doi/10.1103/PhysRevB.34.3820

[17] Blöchl P E 1994 *Phys. Rev. B* **50**(24) 17953–17979 URL http://link.aps.org/doi/10.1103/PhysRevB.50.17953

[18] Kresse G and Furthmüller J 1996 *Phys. Rev. B* **54**(16) 11169–11186 URL http://link.aps.org/doi/10.1103/PhysRevB.54.11169

[19] Kresse G and Furthmller J 1996 *Comp. Mater. Sci.* **6** 15 – 50 URL http://www.sciencedirect.com/science/article/pii/0927025696000080

[20] Kresse G and Joubert D 1999 *Phys. Rev. B* **59**(3) 1758–1775 URL http://link.aps.org/doi/10.1103/PhysRevB.59.1758

[21] Perdew J P and Zunger A 1981 *Phys. Rev. B* **23**(10) 5048–5079 URL http://link.aps.org/doi/10.1103/PhysRevB.23.5048

[22] Makkonen I, Hakala M and Puska M 2005 *J. Phys. Chem. Solids* **66** 1128 – 1135 URL http://www.sciencedirect.com/science/article/pii/S0022369705000521

[23] Hautakangas S, Makkonen I, Ranki V, Puska M J, Saarinen K, Xu X and Look D C 2006 *Phys. Rev. B* **73**(19) 193301 URL http://link.aps.org/doi/10.1103/PhysRevB.73.193301

[24] Mäki J M, Makkonen I, Tuomisto F, Karjalainen A, Suihkonen S, Räisänen J, Chemekova T Y and Makarov Y N 2011 *Phys. Rev. B* **84**(8) 081204 URL http://link.aps.org/doi/10.1103/PhysRevB.84.081204

[25] Segercrantz N, Slotte J, Makkonen I, Kujala J, Tuomisto F, Song Y and Wang S 2014 *Appl. Phys. Lett.* **105** 082113 URL http://scitation.aip.org/content/aip/journal/apl/105/8/10.1063/1.4894473

[26] Tuomisto F, Rauch C, Wagner M R, Hoffmann A, Eisermann S, Meyer B K, Kilanski L, Tarun M C and McCluskey M D 2013 *J. Mater. Res.* **28**(15) 1977–1983 URL http://journals.cambridge.org/article_S0884291413001957

[27] Tuomisto F, Ranki V, Saarinen K and Look D C 2003 *Phys. Rev. Lett.* **91**(20) 205502 URL http://link.aps.org/doi/10.1103/PhysRevLett.91.205502

[28] Børseth T M, Tuomisto F, Christensen J S, Monakhov E V, Svensson B G and Kuznetsov A Y 2008 *Phys. Rev. B* **77**(4) 045204 URL http://link.aps.org/doi/10.1103/PhysRevB.77.045204

[29] Johansen K M, Zubiaga A, Tuomisto F, Monakhov E V, Kuznetsov A Y and Svensson B G 2011 *Phys. Rev. B* **84**(11) 115203 URL http://link.aps.org/doi/10.1103/PhysRevB.84.115203

[30] Chen Z Q, Maekawa M, Yamamoto S, Kawasuso A, Yuan X L, Sekiguchi T, Suzuki R and Ohdaira T 2004 *Phys. Rev. B* **69**(3) 035210 URL http://link.aps.org/doi/10.1103/PhysRevB.69.035210

[31] Chen Z Q, Sekiguchi T, Yuan X L, Maekawa M and Kawasuso A 2004 *J. Phys.: Condens. Matter* **16** S293 URL http://stacks.iop.org/0953-8984/16/i=2/a=035

[32] Chen Z Q, Kawasuso A, Xu Y, Naramoto H, Yuan X L, Sekiguchi T, Suzuki R and Ohdaira T 2005 *J. Appl. Phys.* **97** 013528 (pages 6) URL http://link.aip.org/link/?JAP/97/013528/1

[33] Chen Z Q, Kawasuso A, Xu Y, Naramoto H, Yuan X L, Sekiguchi T, Suzuki R and Ohdaira T 2005 *Phys. Rev. B* **71**(11) 115213 URL http://link.aps.org/doi/10.1103/PhysRevB.71.115213

[34] Chen Z Q, Maekawa M, Kawasuso A, Suzuki R and Ohdaira T 2005 *Appl. Phys. Lett.* **87** 091910 URL http://link.aip.org/link/?APL/87/091910/1

[35] Brauer G, Anwand W, Skorupa W, Kuriplach J, Melikhova O, Moisson C, von Wenckstern H, Schmidt H, Lorenz M and Grundmann M 2006 *Phys. Rev. B* **74**(4) 045208 URL http://link.aps.org/doi/10.1103/PhysRevB.74.045208

[36] Zhi-Quan C, Maekawa M and Kawasuso A 2006 *Chinese Phys. Lett.* **23** 675 URL http://stacks.iop.org/0256-307X/23/i=3/a=042

[37] Chen Z Q, Maekawa M, Kawasuso A, Sakai S and Naramoto H 2006 *J. Appl. Phys.* **99** 093507 URL http://scitation.aip.org/content/aip/journal/jap/99/9/10.1063/1.2194113

[38] Børseth T M, Tuomisto F, Christensen J S, Skorupa W, Monakhov E V, Svensson B G and Kuznetsov A Y 2006 *Phys. Rev. B* **74**(16) 161202 URL http://link.aps.org/doi/10.1103/PhysRevB.74.161202

[39] Neuvonen P T, Vines L, Venkatachalapathy V, Zubiaga A, Tuomisto F, Hallén A, Svensson B G and Kuznetsov A Y 2011 *Phys. Rev. B* **84**(20) 205202 URL http://link.aps.org/doi/10.1103/PhysRevB.84.205202

[40] Janowitz C, Scherer V, Mohamed M, Krapf A, Dwelk H, Manzke R, Galazka Z, Uecker R, Irmscher K, Fornari R, Michling M, Schmeißer D, Weber J R, Varley J B and Van de Walle C G 2011 *New J. Phys.* **13** 085014 URL http://stacks.iop.org/1367-2630/13/i=8/a=085014

[41] Gupta S, Yadav B, Dwivedi P K and Das B 2013 *Mater. Res. Bull.* **48** 3315 – 3322 URL http://www.sciencedirect.com/science/article/pii/S0025540813003401